Published in final edited form as:
Neuroimage. 2011 April 15; 55(4): 1461–1474. doi:10.1016/j.neuroimage.2011.01.064.

Prefrontal pathways target excitatory and inhibitory systems in memory-related medial temporal cortices

Jamie G. Bunce[1] and **Helen Barbas**[1,2]

Jamie G. Bunce: jbunce@bu.edu; Helen Barbas: barbas@bu.edu

[1]Department of Health Sciences, Boston University, Boston, MA

[2]Graduate Program in Neuroscience, Boston University and School of Medicine, Boston, MA

Abstract

The anterior cingulate cortex (ACC), situated in the caudal part of the medial prefrontal cortex, is involved in monitoring on-going behavior pertaining to memory of previously learned outcomes. How ACC information interacts with the medial temporal lobe (MTL) memory system is not well understood. The present study used a multitiered approach to address two questions on the interactions between the ACC and the parahippocampal cortices in the rhesus monkey: 1) What are the presynaptic characteristics of ACC projections to the parahippocampal cortices? 2) What are the postsynaptic targets of the pathway and are there laminar differences in innervation of local excitatory and inhibitory systems? Labeled ACC terminations were quantified in parahippocampal areas TH and TF and a cluster analysis showed that boutons varied in size, with a population of small (≤ 0.97 μm) and large (>0.97 μm) terminations that were nearly evenly distributed in the upper and deep layers. Exhaustive sampling as well as unbiased stereological techniques independently showed that small and large boutons were about evenly distributed within cortical layers in the parahippocampal cortex. Synaptic analysis of the pathway, performed at the electron microscope (EM) showed that while most of the ACC projections formed synapses with excitatory neurons, a significant proportion (23%) targeted presumed inhibitory classes with a preference for parvalbumin (PV+) inhibitory neurons. These findings suggest synaptic mechanisms that may help integrate signals associated with attention and memory.

Keywords

Anterior Cingulate; Parahippocampal Cortex; Non-Human Primate; Parvalbumin; Calbindin; Triple-Labeling Immunohistochemisty

1. Introduction

The anterior cingulate cortex (ACC), situated in the caudal part of the medial prefrontal cortex is involved in monitoring on-going behavior pertaining to memory of previously learned outcomes (MacDonald et al., 2000; Botvinick et al., 2004; Rushworth et al., 2007; 2009 for reviews). Specifically, the ACC is thought to play a role in keeping track of the

Corresponding Author: Helen Barbas, Boston University, 635 Commonwealth Ave., Rm 431, Boston, MA 02215, Tel: 617-353-5036, Fax: 617-353-7567.

consequences of recently made choices (Kennerley et al., 2006). How ACC information interacts with the medial temporal lobe (MTL) memory system is not well understood, but could underlie the integration of attentional context with mnemonic information. Previous studies have reported robust and non-reciprocal projections from the hippocampal formation to the medial prefrontal cortices in macaque monkeys (e.g., Barbas and Blatt, 1995; Munoz and Insausti, 2005). Several reports have shown a projection from ACC to MTL cortices, but there is no information at the synaptic level on the types of neurons innervated in this pathway in monkeys (Carmichael and Price, 1995; Kondo et al., 2005; Apergis-Schoute et al., 2006; Saleem et al., 2008).

The cascade of information flow through the MTL is organized in a laminar manner with multiple cortical areas serving the relational processes necessary for episodic memory (Van Hoesen et al., 1972; Zola-Morgan et al., 1989; Suzuki et al., 1993; Wellman and Rockland, 1997; Burwell and Amaral, 1998; Blatt et al., 2003; Lavenex et al., 2004; Manns and Eichenbaum, 2006; see Suzuki, 2006 and Lavenex and Amaral, 2000 for reviews). The upper layers of the parahippocampal cortices (TH and TF) serve as the cortical foundation of the circuit and originate the principal projection to the rhinal cortices (areas 28, 35, 36), which convey cortical input to the hippocampus (Van Hoesen and Pandya, 1975; Mohedano-Moriano et al., 2007; 2008; Insausti and Amaral, 2008). The deep layers of the parahippocampal cortex receive hippocampal output from the rhinal cortices, including the entorhinal (area 28) and perirhinal (areas 35 and 36) cortices and direct projections to high order association cortices (Swanson and Kohler, 1986; Suzuki and Amaral, 1994a; 1994b; Burwell and Amaral 1998; Lavenex et al., 2002).

Information flow, both to and from the hippocampal formation (HCF), is not a passive process. Signals arriving in the rhinal cortices must overcome robust local inhibition to gain access to the hippocampus (Biella et al., 2002; de Curtis and Paré, 2004; Pelletier et al., 2004). The way by which signals impinge on MTL local circuit dynamics to gain access to hippocampus is unclear (Kloosterman et al., 2003; Kajiwara et al., 2003; Koganezawa et al., 2008). Previous work has shown that laminar-specific pathways linking prefrontal and temporal cortices differ in the size of terminations and interactions with distinct inhibitory systems (Barbas et al., 2005; Germuska et al., 2006; Medalla et al., 2007). Here, we investigated whether the ACC-parahippocampal pathway shows similar synaptic specificity.

We used a multitiered approach to address two unanswered questions surrounding the circuit from the ACC to the parahippocampal cortices: 1) What are the presynaptic characteristics of ACC projections to the parahippocampal cortices? 2) What are the postsynaptic targets of the pathway and are there laminar differences in innervation of local excitatory/inhibitory systems that serve the input and output of this circuit?

2. Methods

2.1 Animals

Studies were conducted on 4 young adult (2.0-3.0 years of age) rhesus monkeys (*Macaca mulatta*) of both sexes weighing 3.2-4.5 kg. Analyses were based on five tracer injections (4 biotinylated dextran amine, 1 lucifer yellow), a sample that was sufficient for statistical analyses (e.g., Hoistad and Barbas, 2008). Experiments were conducted in accordance with NIH Guide for the Care and Use of Laboratory Animals, and every effort was made to minimize pain or distress, and to minimize the number of animals used for each study. A detailed protocol describing all procedures involving animals, including their transport to an imaging center, sedation, anesthesia, surgery, post-surgical care and euthanasia, was approved by the Institute for Animal Care and Use Committee (IACUC) at Boston University, Harvard Medical School (for New England Primate Research Center [NEPRC]),

and Massachusetts General Hospital (for imaging), as being consistent with humane treatment of animals.

Animals were purchased from NEPRC, located in Southborough, MA, where they were housed before and after surgery, and up to euthanasia. The monkeys were maintained on a balanced diet of Purina Monkey Chow supplemented with fresh fruit. The monkeys were housed in individual cages, but in full view of other monkeys to allow for social interactions. Climbing bars and toys were placed in cages to enrich the environment of the animals.

2.2 Brain Imaging

One week prior to surgery, we conducted magnetic resonance imaging (MRI) to guide the injection of neural tracers during surgery. For imaging, the monkey was sedated with propofol (loading dose, 2.5-5 mg/kg intravenous; continuous rate infusion, 0.25-0.4 mg/kg^{-1} min^{-1}) and positioned in a nonmetallic stereotaxic device. MRI was performed with a 3T superconducting magnet (Phillips; or Siemens). A T1 weighted 3D SPGR (TR70, TE6, Flip 45) was obtained through the brain, using a 512 × 384 matrix and a 16 × 16 FOV. Section thickness ranged from 0.65-1 mm with no gaps between successive sections. After imaging the animal was transported back to NEPRC.

2.3 Surgical Procedure to Inject Neural Tracers

One week after imaging we performed surgery to inject neural tracers under general anesthesia at a surgical suite at NEPRC. The monkeys were sedated with ketamine hydrochloride (10-15 mg/kg, intramuscularly), then deeply anesthetized with gas anesthetic (isoflurane), until a surgical level of anesthesia was achieved. Heart rate, muscle tone and respiration were evaluated to maintain a surgical level of anesthesia. Surgery was performed under sterile conditions with the monkey's head held by a stereotaxic apparatus. A craniotomy was made over the site for injection, the dura retracted, and cortex exposed. Tracer injections were made using a microsyringe (5 or 10 μl, Hamilton, Reno, NV, USA) mounted on a microdrive. The bidirectional tracers biotinylated dextran amine (BDA) or lucifer yellow (LY) were of 10kDa molecular weight, optimized for anterograde labeling (Veenman et al., 1992; Reiner et al., 2000). For each injection site, the dye was diluted to 10 mg/ml in distilled water and delivered in 2-4 penetrations spaced 0.5 mm apart, to inject a total volume of 5 μl of dye. After injection of neural tracers, the wound was closed and the animal was given antibiotics and analgesics (buprenex, 0.01 mg/kg) every 12 hrs, or as needed. The animal was monitored until recovery from anesthesia, and then returned to a recovery room at NEPRC.

2.4 Perfusion and tissue processing

After a survival period of 19 days, which allowed the dyes to travel from the injection site to axon terminals, the animal was given an overdose of anesthetic (sodium pentobarbitol, >50 mg/kg, to effect) and perfused with 4% paraformaldehyde, 0.2% glutaraldehyde in 0.1 M phosphate buffer (PB; pH 7.4) at 37° C. The brain was removed and cryoprotected in increasing concentrations of sucrose (15%, 20%, 30% in 0.01 M PBS). The brain was then frozen by immersion in isopentane for rapid and uniform freezing at -70°C and cut in the coronal plane at 50 μm sections in 10 matched series on a freezing microtome. To preserve the ultrastructure, tissue was stored in -20°C in antifreeze solution (30% ethylene glycol, 30% glycerol, 40% 0.05M PB, pH 7.4 with 0.05% azide).

2.5 Immunohistochemistry to visualize boutons labeled with BDA/LY

We used the avidin-biotin (AB) with horseradish peroxidase (HRP) method (Vectastain PK-6100 ABC Elite kit, Vector Laboratories, Burlingame, CA, USA). All assays were

conducted at 4°C. Free floating brain sections were washed in 0.01 M PBS and sections were incubated in 0.05 M glycine and pre-blocked in 5% normal goat serum (NGS) and 5% bovine serum albumin (BSA) with 0.2% Triton X, placed in sodium borohydride (1%) or glycine (0.05%). Sections with BDA were incubated in AB-HRP solution for one hour (1:100 in PBS containing 0.1% Triton-X). The tissue was rinsed and processed using the peroxidase-catalyzed polymerization of diaminobenzidine (DAB; 0.05% DAB, and 0.004% H_2O_2 in PBS) for 2-3 min (DAB kit, Vector or Zymed Laboratories Inc., South San Francisco, CA, USA). Sections with fluorescent tracer were incubated overnight in antibody against LY (1:800, in PBS, 1% NGS, 1% BSA, 0.1% Triton-X; rabbit polyclonal, Molecular Probes), followed by incubation in secondary biotinylated goat anti-rabbit IgG (1:200, for 2 hrs; Vector), then in AB-HRP and DAB as previously described. Following processing, sections were rinsed, mounted on gelatin-coated slides, dried, dehydrated in graded alcohols, cleared in xylenes and coverslipped with Permount. Every other section was counterstained with thionin (Sigma, St. Louis, MO, USA) to define areal and laminar boundaries. We used the same procedure to process BDA tissue for electron microscopy, but with 0.025% Triton-X to preserve the ultrastructure.

2.6 Triple pre-embedding immunohistochemical labeling for EM

Triple labeling pre-embedding immunohistochemistry for serial electron microscopy was used to investigate pathway interactions of multiple pre- and postsynaptic elements. Pre-embedding labeling has the advantage of strong, specific labeling due to easier penetration of reagents in free-floating sections, before they are dehydrated and embedded in resin. We used triple immunohistochemical methods to label neural tracers with DAB (above) and parvalbumin (PV) or calbindin (CB) neurons with either silver-enhanced gold-conjugated or tetramethylbenzidine (TMB) labeled secondary antibodies. These methods show distinct labeling at the EM: DAB appears as a dark uniform precipitate, silver-enhanced gold particles as circular clumps of variable size, and TMB as rod-shaped crystals (e.g., Pinto et al., 2003; Gonchar and Burkhalter, 2003; Moore et al., 2004; Zikopoulos and Barbas, 2007).

After labeling fibers with DAB, sections were incubated in AB blocking reagent to prevent cross-reaction with TMB. For BDA labeled tissue, sections were co-incubated overnight in the primary antibodies for PV (1:2,000, rabbit polyclonal) and CB (1:2,000 mouse polyclonal; Swiss Antibodies, Bellinzona, Switzerland) and then in biotinylated anti-mouse IgG, followed by AB-HRP. Sections were post-fixed in 6% glutaraldehyde with 2% paraformaldehyde using a variable wattage microwave (3-6 min at 150W in the Biowave; Ted Pella, Redding, CA, USA) until the fixative temperature reached 30°C. Gold labeling was intensified with silver (6-12 min; IntenSE M kit, Amersham), which results in aggregates of gold particles of variable sizes. Sections were processed for TMB, then stabilized with DAB-cobalt chloride solution. In control experiments we omitted primary antibodies to test the specificity of secondary antibodies and used the AB blocking kit prior to AB binding to test the specificity of labeling.

After labeling we cut small pieces of cortex (all layers) with anterograde label in areas TH and TF. These pieces were post-fixed in osmium, rinsed, dehydrated in increasing concentrations of ethanol (50-100%), stained with 1% uranyl acetate (EM Sciences, Hatfield, PA, USA) infiltrated with propylene oxide, and flat embedded in LX112 (Ladd Research Industries, Williston, VT, USA) using aclar plastic (Ted Pella, Redding, CA, USA). Pieces of aclar-embedded tissue were cut and re-embedded in resin blocks and sectioned at 50 nm with a diamond knife (Diatome USA, Hatfield, PA, USA) using an ultramicrotome (Ultracut, Leica, Wein, Austria). Serial ultrathin sections were collected on single slot pioloform-coated grids.

2.7 Data analysis

2.7.1 Population Analysis—Photomicrographs of labeled boutons in the parahippocampal cortices were captured at the light microscope (LM) using a high resolution CCD camera (Olympus DP70). We acquired image stacks of multiple focal planes to create pictures through the entire thickness of the sections in the z-axis using ImageJ (v. 132j for Windows; NIH, USA) as described (Medalla and Barbas, 2006; Zikopoulos and Barbas, 2006). To obtain population estimates of bouton size we captured images at high magnification (1,000×) of >3 random sites within a region of anterograde label in the upper and deep layers of areas TH and TF. Within each stack of images, we manually traced the profile of each labeled bouton to measure the major diameter using ImageJ.

2.7.2 Quantitative mapping: LM analysis—We collected all data quantitatively using exhaustive sampling or unbiased stereologic procedures and analyzed them using conventional statistics, or multidimensional analyses when it was necessary to consider multiple factors simultaneously (Dombrowski et al., 2001; Hilgetag et al., 2002).

Labeled boutons in MTL were mapped in precise register with respect to anatomic landmarks using a work station with an encoded microscope stage interfaced to a computer using commercial software (Neurolucida, Microbrightfield). Exhaustive sampling of labeled boutons was achieved by using a meander scan to systematically progress through the entirety of each area. The exhaustive sampling data included bouton frequencies and calculations for area, which were used to calculate the relative density of boutons per unit area (mm^2). We estimated bouton density in all areas using exhaustive sampling or stereologic procedures aided by a semi-automated system (StereoInvestigator, Microbrightfield), as described (e.g., Germuska et al., 2006; Zikopoulos and Barbas, 2007; Medalla et al., 2007). For each area, a minimum of three evenly spaced sections were selected using systematic random sampling to count boutons in different laminar compartments (superficial layers I-III and deep layer IV-VI). The stereological data included volume calculation for each laminar group, which takes into consideration the area of the layer and thickness of each section. We counted boutons using an optical disector restricted to the central fraction of the tissue thickness (11 μm). The top and bottom of each section (minimum 2 μm for 15 μm sections after shrinkage) thus were used as guard zones to avoid error due to possible uneven tissue sectioning. The actual thickness of mounted sections was measured by the program at each counting site. The counting frame/disector size (area 40 × 40 μm; height = 11 μm) and grid spacing (ranging from 100 × 100 μm to 400 × 400 μm) were set to employ a sampling fraction to yield a coefficient of error of ≤ 10%), as recommended (see Gundersen et al., 1988; Howard and Reed, 1998 for review). The stereologic analysis yielded estimates of the total number of boutons in each laminar group and the volume of the laminar group examined. The volume estimates along with the total estimates of boutons were used to calculate the density of boutons per unit volume (mm^3). We normalized data to account for variability of labeling due to differences in the size of the injections. The relative density of labeled boutons in each area was expressed as a percentage of the total density of boutons mapped in the MTL cortices for each injection site. The relative laminar density of small and large boutons in each area was expressed as a percentage of the total density of boutons within a laminar group in each area for each injection site. Densities within areas TH and TF were subsequently collapsed to express an omnibus relative laminar density for the superficial and deep layers of the parahippocampal cortices. This was expressed as the percentage of small and large boutons within the superficial (I-III) or deep (IV-VI) layers for each injection and then averaged across cases. Numerical data were transferred to a database (MS Excel).

2.7.3 Correlated LM-EM analyses—We used a combined LM-EM approach to study synapses of the ACC-parahippocampal pathway (e.g., Barbas et al., 2003; Medalla and Barbas, 2010). Briefly, after tissue processing to view tracer label, we mounted brain sections with labeled axon boutons in the areas of interest on glass slides, viewed them while wet, captured images of labeled sites with a CCD camera, and cut small blocks of tissue containing label, osmicated and embedded them for ultrathin sectioning. We then cut the blocks of tissue into ultrathin sections (Ultracut, Leica) in series to reconstruct labeled synapses, as described briefly below and in previous studies (e.g., Zikopoulos and Barbas, 2006; 2007; Germuska et al., 2006; Medalla et al., 2007; Bunce and Barbas; 2008).

We viewed fields with labeled boutons at the EM (100CX, JEOL, Peabody, MA, USA) and captured images using a digital camera (ES1000W, Gatan, Pleasanton, CA, USA) at a magnification of 6,000-33,000×. We determined synapse type, and measured synapses from the images using image analysis systems (ImageJ; Reconstruct, Fiala; 2005). For serial reconstruction, we first aligned images to correct misalignment caused by serial sectioning and imaging of the tissue, and used the software to apply transformations expressed explicitly as a set of rotations, scaling and stretches, or implicitly by specifying a set of corresponding points in contiguous images. The points were then aligned using a selection of linear and non-linear transformations. To ensure that the generated 3D object was geometrically accurate, the dimensions of each serial image were calibrated. We photographed a diffraction grating at the same time as the series to calibrate the x and y axes from the specified grid spacing. Section thickness was measured by the method of cylindrical diameters (Fiala and Harris, 2001). We traced pre- and postsynaptic elements and generated a 3D reconstruction of an object represented in the aligned image sections. The boundaries of an object were defined by contours for each section. Once all object contours were defined in serial sections, the program generated a 3D Virtual Reality Modeling Language object.

2.7.4 Quantitative analysis of labeled synapses: EM—Images of sites containing labeled synapses were imported in Reconstruct to mark synapses by type, cross-sectional area and synaptic length (e.g., Barbas et al., 2003; Germuska et al., 2006). Conventional (e.g., ANOVA), or multidimensional statistical analyses were performed on data as described (Medalla and Barbas, 2006; Dombrowski et al., 2001; Hilgetag et al., 2002).

We used classic criteria for identifying synapses and profiles (Peters et al., 1991; Carr and Sesack, 1998; Peters and Palay, 1996): by the aggregation of synaptic vesicles in the presynaptic bouton; rigid apposition of the presynaptic and postsynaptic membranes and widening of the extracellular space and the presence of pre- and postsynaptic membrane specializations. Asymmetric synapses (type I) have thickened postsynaptic densities and rounded vesicles; and symmetric (type II) synapses have thin postsynaptic densities and pleomorphic vesicles. Pyramidal neurons have dendrites with spines, which receive the vast majority of synapses. Inhibitory neurons in the cortex have smooth or sparsely spiny dendrites and receive synapses mostly on the shafts of their dendrites. Inhibitory neurons form symmetric synapses with a variety of elements from other neurons. Axon terminals are >0.1 μm in diameter and contain synaptic vesicles, and often have mitochondria. Dendritic shafts contain mitochondria, microtubules and/or rough endoplasmic reticulum, while dendritic spines lack these organelles.

2.7.5 2D and 3D EM analysis—For 2D analysis at the EM we exhaustively sampled all labeled boutons from series of sections. We used ImageJ to measure the major diameter of labeled boutons at the level of the synapse. For 3D analysis, we used series of 100 sections and identified all labeled boutons in the series. We followed and photographed each bouton throughout adjacent serial sections (20-80 sections) for each synapse and reconstructed

labeled boutons and their postsynaptic targets using the program Reconstruct. We traced pre- and postsynaptic elements and generated a 3D reconstruction of an object represented in the aligned image sections. The boundaries of an object were defined by contours for each section. Once all object contours were defined in serial sections, the program generated a 3D Virtual Reality Modeling Language object.

2.7.6 Statistics—Data sets were compared using analysis of variance (ANOVA) or multidimensional statistical analyses. Linear regression was conducted using least squares. All statistical analyses were performed using SPSS (XVI for Windows). To test the reliability of the sampling method we examined if the proportion of total boutons sampled in the superficial and deep layers of each area of interest fell within ~10% of the proportions calculated during exhaustive sampling and stereological quantification (data not shown).

2.8 Photography

Photomicrographs were captured using a CCD camera mounted on an Olympus Optical microscope (BX60) connected to a personal computer using a commercial imaging system (NeuroLucida, Virtual Slice software, MicroBrightfield, Williston, VT, USA) or using a digital camera (ES1000W, Gatan, Pleasanton, CA, USA) at the EM. For the population analysis, we acquired image stacks of several focal planes in each area of interest, resulting in pictures with high depth of field focused throughout the z axis extent. Stacks were then combined to create a composite image using ImageJ, scaled, and all labeled boutons were traced. ImageJ output was exported to a database in Excel. For presentation, images were imported into Adobe Photoshop CS for adjustment of overall brightness and contrast but were not retouched. Images were assembled in ACD Canvas X.

3. Results

3.1 Nomenclature

The nomenclature used is based on the maps of Seltzer and Pandya (1978) and Suzuki and Amaral (1994a) and is similar to that used previously (Rempel-Clower and Barbas, 2000; Hoistad and Barbas, 2008). Our analysis in the medial temporal lobe included the parahippocampal cortices (areas TH and TF) and the borders were consistent with the maps of Suzuki and Amaral (1994a).

3.2 Injection sites

Data were obtained from injections of BDA and LY in area 32 (n=5 injection sites in 4 cases). Injection sites from three cases with BDA in area 32 are presented with the corresponding distribution of labeled terminals in Figures 2 and 3. In all cases the tracer occupied both superficial and deep layers. In case AY the corona of the injection impinged on the medial part of area 9. Parahippocampal cortices have few, if any, connections with the medial portions of area 9 (Barbas et al., 1999; Kondo et al., 2005), suggesting that this region did not contribute significantly to the projections seen in areas TH and TF.

Labeled axons from area 32 were distributed throughout the anterior-posterior extent of the parahippocampal cortices. Initial observations revealed labeled *terminaux* and *en passant* boutons present in the superficial (I-III) and deep (IV-VI) layers of both areas TH and TF (Figures 2, 3). The distribution of BDA labeled ACC terminations is presented in Figure 2.

3.3 Presynaptic size of ACC terminations in the parahippocampal cortex: LM analysis

Physiologic and computational studies have shown that large boutons have more synaptic vesicles and greater synaptic efficacy because of increased probability of neurotransmitter release and increased likelihood of multivesicular release with each action potential

(Rosenmund and Stevens, 1996; Murthy et al., 1997; Walmsley et al., 1998; Stevens, 2003). We thus measured the size of anterogradely labeled boutons in the parahippocampal cortices at the LM. To quantify the size of small and large terminations, and thereby better assess the potential salience of the ACC signal in the parahippocampal cortices, we conducted a population analysis at the LM, and measured the size of anterogradely labeled boutons from area 32. We traced and measured the major diameters of boutons from a large sample of terminations in the superficial (n=4,200) and deep (n=3,298) layers in parahippocampal regions TH/TF. A k-means cluster analysis (SPSS 16.0) sorted ACC terminations into large and small populations based on the major diameters of boutons (Figure 4). Initially we performed cluster analyses on boutons from the individual cases. There were no significant differences among clusters from individual cases (ANOVA yielded no significant effects of case or layer on bouton major diameter F's<1.0; P's>0.05; data not shown), so we pooled data on bouton diameters and performed an overall cluster analysis. Large boutons centered around 1.41 μm (sd ± 0.28) and small boutons at 0.76 μm (sd ± 0.21; F[1,7496]=12688, p<0.001, Figure 4C). Analysis by laminar groups showed that in the superficial layers, large boutons centered around 1.4 μm (sd ± 0.29) and small boutons at 0.74 μm (sd ± 0.22; F[1,4198]=6846, p<0.001; data not shown). In the deep layers, large boutons centered around 1.4 μm (sd ± 0.26), and small boutons around 0.78 μm (sd ± 0.2; F[1,3296]=5998; p<0.001; data not shown).

Accordingly, we used these data to compute a criterion threshold (overall small cluster center [0.76 μm] + standard deviation [0.21]) to classify the sample of boutons captured during the 2D population analysis. Based on this threshold, boutons with major diameters ≤0.97 μm were classified as small and those >0.97 μm were classified as large. Based on these classifications, small and large boutons were nearly evenly distributed in both the superficial (small 53.4% ± 1.6; large 46.6% ± 1.6) and deep (small 49.5% ± 5.6; large 50.5% ± 5.6) layers of the parahippocampal cortices (Figure 4D).

3.4 Density and pattern of ACC terminations in the parahippocampal cortices

We next investigated the density and mapped the distribution of small (≤0.97 μm) and large diameter (>0.97 μm) ACC terminations in the superficial (I-III) and deep (IV-VI) layers of the parahippocampal cortices using exhaustive sampling and unbiased stereological techniques. In general, there was no effect of region of interest (area TH vs. TF), laminar group (superficial vs. deep) or bouton size (large vs. small) indicating that both large and small boutons were evenly distributed throughout the superficial and deep layers of areas TH and TF (F's<1.2; P's>0.25; Figure 4E). Therefore we collapsed the data across areas and found a small preference for ACC terminations in the superficial (53.3 ± 6.6%) compared to the deep (46.7 ± 6.6%) layers of the parahippocampal cortices (Figure 4F). The proportion of large to small boutons was similar to that calculated during the initial 2D analysis of bouton diameters conducted at the LM which yielded approximately even ratios of large to small boutons in the superficial (large=53.5% ± 7.0; small=46.5% ± 7.0) and deep layers (large=51.5% ± 7.8; small=48.6% ±7.8), with a slightly higher tendency for large boutons overall (compare Figures 4D and 4F).

3.5 Synaptic characteristics of ACC terminations in the parahippocampal cortex: EM analysis

In addition to widespread reach, evident by terminations in both the upper and deep layers of both parahippocampal areas, the high incidence of large boutons suggests that the ACC can exert a powerful postsynaptic effect within the MTL. We investigated this issue at the synaptic level to characterize the pre- and postsynaptic targets of the circuit using correlated LM-EM combined with immunohistochemistry to label postsynaptic sites (Figure 5). Data

derived from the LM guided subsequent analysis at the EM. We employed triple labeling to view the tracer and two classes of inhibitory neurons expressing PV or CB.

We imaged 73 labeled boutons in the parahippocampal cortex. Six boutons were multisynaptic resulting in a total of 79 synapses included in the analyses. Forty-eight boutons were captured in the upper layers and 25 in the deep layers of the parahippocampal cortex. Congruent with observations at the LM, the majority of presynaptic terminals (66%) were *en passant*. All boutons studied formed asymmetric synapses and were presumed to be excitatory. Nineteen percent of the synapses were perforated (60% were found in the upper and 40% in the deep layers). Perforated synapses have segmented PSDs and are proposed to be more efficacious than non-perforated synapses (Greenough et al., 1978; Sirevaag and Greenough 1985; Geinisman et al., 1987; Ganeshina et al., 2004a).

Initially we performed a 2D EM analysis by measuring bouton major diameters at the synaptic level. Cluster analysis on bouton major diameters in parahippocampal area TF captured at the EM showed that small boutons clustered around 0.82 μm (sd ± 0.15) and large boutons centered around 1.3 μm (sd ± 0.2; $F[1,71]=154$, $p<0.001$; Figure 6A). This analysis confirmed the findings calculated at the LM (compare with Figure 4C). Using the small bouton cluster (center [0.82 μm] + sd [0.15]) as a threshold criterion, we classified boutons with major diameters ≤0.97 μm as small and those >0.97 μm as large. This analysis revealed a comparable distribution of small (42.5%) and large (57.5%) boutons in area TF (Figure 6B). The distribution of small and large boutons was even in the superficial (small: 50.0%; large: 50.0%) and tilted towards large boutons in the deep layers (small: 36.0%; large: 64.0%). Bouton major diameters most frequently fell between 0.5 μm and 1.5 μm, similar to diameters calculated at the LM (compare Figure 6E with 4A & 4B). Approximately one quarter of large boutons (23.8%) formed perforated synapses with their postsynaptic targets compared to 16.0% of perforated synapses formed by small boutons.

We then performed a 3D EM analysis by aligning 22 series of images with labeled boutons in the parahippocampal region TF obtaining 18 complete reconstructions of terminal boutons that formed 21 synapses (n=10 boutons and 12 synapses in the upper layers; n=8 boutons and 9 synapses in the deep layers). In addition to presynaptic terminals, we reconstructed 19 spines and segments of 2 dendrites which were postsynaptic targets of labeled boutons. We performed a cluster analysis on volumes derived from 3D reconstructions of boutons captured in area TF (Figure 7) and found that small boutons centered at 0.25 μm^3 (sd ± 0.1) and large boutons at 0.57 μm^3 (sd ± 0.12; $F[1,18]=39.78$, $p<0.001$; Figure 6C). Using the small bouton cluster (center [0.25 μm^3] + sd [0.1]) as a threshold criterion, we classified boutons with volumes ≤0.36 μm^3 as small and those with volumes that exceeded this criterion as large. Based on these classifications, we observed a distribution of large (61.1%) and small (38.9%) boutons in parahippocampal area TF (Figure 6D). Small and large boutons were overall nearly evenly distributed (superficial small: 60.0%; large: 40.0% and deep small: 37.5%; large: 62.5%). These results lend further support to the finding that the ACC area 32 originates projections which terminate in two populations of boutons with large and small presynaptic elements.

3.6 Postsynaptic targets in the parahippocampal cortex

Of the 73 boutons captured in the 2D and 3D analyses, 6 were multisynaptic, resulting in a total of 79 postsynaptic elements analyzed. Most (77%) of the labeled ACC terminations formed synapses with unlabeled spines from presumed excitatory neurons of which 16% were perforated. Overall, slightly more large boutons (60.7%) formed synapses with putative excitatory postsynaptic targets than small boutons (39.3%). A significant number (23%) of ACC terminations formed synapses with putative inhibitory targets (Figures 8A) of which 28% were perforated. Most (72%) of the inhibitory targets were found in the upper

layers and the remaining (28%) were found in the deep layers of parahippocampal cortex. More large boutons (55.6%) formed synapses with inhibitory postsynaptic elements than small boutons (44.4%).

Most (61%) putative inhibitory targets were dendritic shafts of PV+ neurons or spines from PV+ dendrites, presumed to be emanating from sparsely spiny inhibitory neurons (Figure 5A & 5B, 8A). While we did observe robust CB+ signal in the tissue, only 5.5% of area 32 boutons targeted dendrites of CB+ neurons (Figure 5D, 8A). A third (33%) of the labeled ACC terminations formed synapses with smooth, unlabeled, dendritic shafts. In primates, cortical inhibitory neurons fall into three non-overlapping neurochemical classes (PV, CB, and calretinin [CR]), which suggests that the smooth, unlabeled dendrites could have belonged to CR+ inhibitory neurons (Figure 5C, 8A) which were not labeled in the study, or to PV+ or CB+ neurons that were not completely labeled.

3.7 Relationship between presynaptic and postsynaptic elements

We next examined the relationship between presynaptic and postsynaptic elements of the pathway from ACC to parahippocampal cortices. We quantified several features using the 3D reconstructions including bouton volume, postsynaptic density (PSD) area and spine volume. Regression analyses showed that large terminals were associated with large spines based on 3D volumes that were proportional to spine volumes (R^2=0.36 p=0.02; Figure 6F). There was a positive relationship between bouton volume and PSD area, so that large terminals were associated with large PSDs (R^2=0.38; p=0.01; Figure 5G), and large spines were associated with large PSD areas (R^2=0.87; p<0.0001; Figure 5H). These relationships are consistent with previous studies of prefrontal pathways to superior temporal auditory cortices (Germuska et al., 2006). Thus, the size of the specific site of synaptic action appears to be proportional to the size of the postsynaptic element.

4. Discussion

We employed a tiered, multidimensional approach to measure quantitatively and map the distribution of ACC terminations and their postsynaptic targets in the parahippocampal cortices. Using three independent methods at the LM and EM as well as 2D and 3D analyses, we found that ACC terminations in the parahippocampal cortices were comprised of small and large boutons, which were nearly evenly distributed in the upper and deep layers or areas TH and TF. Pre- and postsynaptic analyses showed that the majority of targets were unlabeled spines of putative excitatory neurons. However, a significant number of synapses were formed with local presumed inhibitory targets most of which were PV+. These results pertain to the issue of how attentional and contextual signals are integrated with mnemonic information in primates, as elaborated below.

4.1 Laminar and areal distribution of ACC terminations in the parahippocampal cortices

Informational flow through MTL cortices is organized in a laminar manner with hippocampal bound signals cascading through the superficial MTL layers while hippocampal output is conveyed through the deep layers towards association cortices. ACC terminations were nearly evenly distributed in the upper and deep layers of the parahippocampal areas TH and TF with only a slight preference for the upper layers. This finding is in general accord with previous studies showing that the organization of prefrontal projections to temporal regions is best predicted by cortical structure (see Figure 4C; Rempel-Clower and Barbas, 2000). Thus, the ACC is positioned to impinge on the mnemonic circuits leading both to and from the hippocampal formation. Terminations originating from ACC included both small (≤0.97 μm) and large (>0.97 μm) boutons, which were about evenly distributed in the upper and deep layers. Previous studies of prefrontal-

temporal pathways described populations of small and large boutons which were laminar specific, with small boutons terminating mostly in the upper layers while large boutons were predominantly found in the middle-deep layers of auditory association cortex (Germuska et al., 2006). In the present study, the ratio of small to large boutons was close to 50:50 in the superficial and deep layers with only a slight bias for more large boutons in the deep layers. This evidence suggests that a robust attentional signal from the ACC (Schall et al., 2002) reaches the parahippocampal cortices serving the integration of sensory and mnemonic signals. While the range in size of ACC terminations was nearly identical to that observed in the ACC projection to auditory association cortices (e.g., Medalla et al., 2007), or to other prefrontal cortices (Medalla and Barbas, 2009; 2010), the frequency of large terminations was much higher in the ACC-parahippocampal pathway than in the ACC projection to auditory cortex. Thus, while the presence of small and large boutons may be a general feature of ACC projections, the present findings suggest that the prevalence of large boutons varies with respect to area of termination.

4.2 Projections from the ACC are positioned to knock loudly in the parahippocampal cortices

Through widely distributed terminations in both the upper and deep layers of the parahippocampal cortices, ACC area 32 is positioned to impinge on the neurons that transfer information to and from the rhinal cortices, which are the cortical gateway to the hippocampus. Importantly, the high proportion of large boutons suggests that the ACC signal in the MTL is robust. This is based on physiologic and computational evidence showing that large boutons have more synaptic vesicles, which is correlated with increased probability of neurotransmitter release, and the likelihood of multivesicular release with each action potential, resulting in greater synaptic efficacy (Rosenmund and Stevens, 1996; Murthy et al., 1997; Walmsley et al., 1998; Stevens, 2003). It is interesting to note that large boutons formed the majority (67%) of the perforated synapses, known to be extremely efficacious due to an abundance of AMPA receptors (Ganeshina et al., 2004b). In addition, the size of pre- and postsynaptic elements was related: bouton volume and spine volume as well as bouton volume and PSD area were significantly correlated suggesting a strong functional relationship in the pathway. These findings suggest that synapses composed of large boutons appear to be a component of a specialized mechanism incorporating 1) a more synaptically efficient presynaptic site (Germuska et al., 2006); 2) and a proportionally adapted postsynaptic element.

4.3 Interactions between ACC and parahippocampal inhibitory mechanisms

Most (77%) postsynaptic targets were spines emanating from presumed excitatory neurons, but a significant proportion (23%) of ACC terminations formed synapses with inhibitory postsynaptic elements, the majority of which were PV+. In the neocortex in primates there are three neurochemically distinct classes of inhibitory neurons, PV, CB and CR (Hendry et al., 1989; DeFelipe et al., 1989; DeFelipe, 1997). PV and CB neurons are most prevalent in the middle-deep and the upper cortical layers, respectively (see Figure 8B & 8C), and target mostly principal (pyramidal) cells (DeFelipe et al., 1989; reviewed by Somogyi et al., 1998). In general, the proportion of ACC terminations forming synapses with inhibitory targets in the parahippocampal cortices was higher than in pathways to superior temporal auditory areas (Germuska et al., 2006, Medalla et al., 2007). The preference for PV+ inhibitory elements and the paucity of CB+ targets was similar to that reported in the ACC pathway to superior temporal auditory cortices (Medalla et al., 2007). These findings suggest a common mechanism for achieving inhibitory control in temporal cortices.

Our findings suggest that the ACC is positioned to exert a powerful effect on local inhibitory neurons in the MTL. This hypothesis is based on the fact that, with the exception of sparse

inter-areal projections to adjacent structures (Tomioka and Rockland, 2007), no long-distance corticocortical inhibitory projections have been described in monkeys. Inhibitory control in primates may therefore be exercised via feed-forward excitatory (glutamatergic) projections acting on local inhibitory neurons (Figure 8D). Conversely, long distance projections may terminate on local principal neurons, which in turn synapse with local inhibitory neurons resulting in indirect inhibitory control. While the present study cannot test for indirect inhibitory control, our results show that the predominant inhibitory target of ACC terminations in the parahippocampal cortices are PV+ presumed inhibitory neurons, whose functional significance is elaborated below (Figure 8E).

4.4 ACC-parahippocampal mechanisms and MTL information transfer

Information flow through MTL cortices is not a passive process. Sensory information arriving in the upper layers of the rhinal cortices must overcome robust inhibition to gain access to the hippocampal formation (Biella et al., 2002; de Curtis and Paré, 2004; Pelletier et al., 2004). How might signals overcome this wall of inhibition? Synchronous theta (4-12 Hz) activity in the medial prefrontal cortex (mPFC) is thought to facilitate information transfer in the rhinal cortices thereby overcoming the rhinal wall of inhibition (Paz et al., 2007; Paz et al., 2008). While the specific anatomical substrate is unclear, synaptic analysis in the rat showed that mPFC terminations form synapses with both excitatory and with unidentified inhibitory postsynaptic targets in the rhinal cortices (Apergis-Schoute et al., 2006). The present results provide two and potentially synergistic mechanisms by which the ACC can mediate information transfer within the parahippocampal cortices. First, through a widespread distribution and a high proportion of large and synaptically efficient boutons, the ACC is positioned to loudly knock on postsynaptic targets within the parahippocampal cortices and thereby impinge on local inhibitory tone. Second, the high incidence of terminations forming synapses with PV+, putative inhibitory neurons, positions the ACC to impinge on parahippocampal inhibitory dynamics thus affecting the neuronal coherence necessary for information transmission within the circuit (see Fries, 2005 for review).

Increasing evidence points to a specialized role that PV+ inhibitory neurons play in the generation of gamma oscillations (30-100 Hz) within sensory cortices, MTL and related regions (Tamas et al., 2004; Fuchs et al., 2007; Klausberger and Somogyi, 2008; Middleton et al, 2008; Mann and Mody, 2010; Ellender and Paulsen, 2010; Otte et al., 2010; see Wang, 2010 for review). In various cortical systems, gamma activity is thought to underlie the integration of signals within neuronal networks (Gray and Singer, 1989; Chrobak and Buzsaki, 1998). Recent evidence has shown that gamma and theta oscillations can facilitate information transfer within local neocortical circuits and between distributed neural regions, respectively (Makeig et al., 2004; Sohal et al., 2009; von Stein and Sarnthein, 2000). To this end, there is a growing body of evidence that attention can modulate gamma as well as theta oscillations and synchronize prefrontal and MTL cortices (Fries et al., 2001; Wang et al., 2005; Buia and Tiesinga, 2006; Womelsdorf et al., 2006; Borgers et al., 2008; Womelsdorf and Fries, 2007 for review), which is thought to be the physiological substrate for updating distributed areas of the circuit with behavioral context (Makeig et al., 2004; Fan et al., 2007). It follows then that gamma and theta oscillations are highly correlated with memory performance in primates (Fell et al., 2001; Sederberg et al., 2003; Canolty et al., 2006; Jutras et al., 2009; Jutras and Buffalo, 2010), and specifically with working memory load (Howard et al., 2003).

In the parahippocampal cortices, gamma oscillations are correlated with hippocampal sharp wave/ripple complexes, which further supports a proposed role in the transfer of mnemonic information within the MTL (Le Van Quyen et al., 2010). By targeting PV+ neurons, the ACC is positioned to impinge on gamma dynamics and thereby affect neuronal communication within the network serving information transfer to and from the rhinal

cortices. Through this pathway the ACC may thus play a key role in determining what information accesses the hippocampus for memory formation as well as what newly generated memories are directed to neocortical sites. Thus, in light of the present results, the interaction between the ACC and the parahippocampal cortices could be the anatomical foundation by which physiological dynamics update emerging memories with contextual information pertaining to the outcome of ongoing behavior.

5. Conclusion

The present study showed that small and large terminations from ACC area 32 were about evenly distributed in the upper and deep layers of the parahippocampal cortices. This evidence suggests that a robust attentional signal from ACC impinges on the parahippocampal cortices. ACC boutons predominantly formed synapses with spines of putative excitatory neurons, though a significant number of terminations targeted local inhibitory elements, the majority of which were PV+ putative inhibitory neurons. This evidence suggests that the ACC is positioned to affect mnemonic information transfer within the MTL, possibly through synchronous oscillatory network activity. Subsequent physiologic studies are necessary to determine whether the ACC facilitates information transfer through the parahippocampal cortices.

Acknowledgments

We thank Dr. Alan Peters for EM consultation, Dr. Ron Killiany for MRI assistance, Dr. Angela Carville for veterinary care, Linda Fernsten for surgical assistance, Dr. Claus Hilgetag for suggestions pertaining to statistical analyses, Marcia Feinberg for outstanding EM technical assistance, as well as Dr. Basilis Zikopoulos and Dr. Maria Medalla for helpful discussions of the manuscript.

Supported by: NIMH (NRSA #1F32MH087076), NIH grants (NIMH and NINDS), and NSF (CELEST).

Abbreviations

ACC	Anterior cingulate cortex
ANOVA	Analysis of variance
AB	Avidin-biotin
BDA	Biotinylated dextran amine
BSA	Bovine serum albumin
CB	Calbindin
CR	Calretinin
DAB	Diaminobenzidine
EM	Electron microscope
HCF	Hippocampal formation
HRP	Horseradish peroxidase
IACUC	Institute for animal care and use committee
LM	Light microscope
LY	Lucifer yellow
MRI	Magnetic resonance imaging
MTL	Medial temporal lobe

mPFC	medial prefrontal cortex
NEPRC	New England Primate Research Center
NGS	Normal goat serum
PV	Parvalbumin
PB	Phosphate buffer
PBS	Phosphate buffered saline
PSD	Postsynaptic density
TMB	Tetramethylbenzidine

References

Apergis-Schoute J, Pinto A, Paré D. Ultrastructural organization of medial prefrontal inputs to the rhinal cortices. Eur J Neurosci. 2006; 24(1):135–144. [PubMed: 16800862]

Barbas H, Blatt GJ. Topographically specific hippocampal projections target functionally distinct prefrontal areas in the rhesus monkey. Hippocampus. 1995; 5:511–533. [PubMed: 8646279]

Barbas H, Ghashghaei H, Dombrowski SM, Rempel-Clower NL. Medial prefrontal cortices are unified by common connections with superior temporal cortices and distinguished by input from memory-related areas in the rhesus monkey. J Comp Neurol. 1999; 410:343–367. [PubMed: 10404405]

Barbas H, Medalla M, Alade O, Suski L, Zikopoulos B, Lera P. Relationship of prefrontal connections to inhibitory systems in superior temporal areas in the rhesus monkey. Cereb Cortex. 2005; 15:1356–1370. [PubMed: 15635060]

Barbas H, Saha S, Rempel-Clower N, Ghashghaei T. Serial pathways from primate prefrontal cortex to autonomic areas may influence emotional expression. BMC Neurosci. 2003; 4:25. [PubMed: 14536022]

Biella G, Uva L, de Curtis M. Propagation of neuronal activity along the neocortical-perirhinal-entorhinal pathway in the guinea pig. J Neurosci. 2002; 22:9972–9979. [PubMed: 12427854]

Blatt GJ, Pandya DN, Rosene DL. Parcellation of cortical afferents to three distinct sectors in the parahippocampal gyrus of the rhesus monkey: an anatomical and neurophysiological study. J Comp Neurol. 2003; 466:161–179. [PubMed: 14528446]

Borgers C, Epstein S, Kopell NJ. Gamma oscillations mediate stimulus competition and attentional selection in a cortical network model. Proc Natl Acad Sci USA. 2008; 105(46):18023–18028. [PubMed: 19004759]

Botvinick MM, Cohen JD, Carter CS. Conflict monitoring and anterior cingulate cortex: an update. Trens Cog Sci. 2004; 8(12):539–546.

Buia C, Tiesinga P. Attentional modulation of firing rate and synchrony in a model cortical network. J Computat Neurosci. 2006; 20(3):247–264.

Bunce, JG.; Barbas, H. Anterior cingulate projections to medial temporal cortices are positioned to modulate mnemonic output. Washington: Society for Neuroscience; 2008. Abstract, 2008 Online

Burwell RD, Amaral DG. Perirhinal and postrhinal cortices of the rat: interconnectivity and connections with the entorhinal cortex. J Comp Neurol. 1998; 391:293–321. [PubMed: 9492202]

Canolty RT, Edwards E, Dalal SS, Soltani M, Nagarajan SS, Kirsch HE, Berger MS, Barbaro NM, Knight RT. Gamma power is phase-locked to theta oscillations in human neocortex. Science. 2006; 313(5793):1626–1628. [PubMed: 16973878]

Carmichael ST, Price JL. Limbic connections of the orbital and medial prefrontal cortex in macaque monkeys. J Comp Neurol. 1995; 363:615–641. [PubMed: 8847421]

Carr DB, Sesack SR. Callosal terminals in the rat prefrontal cortex: synaptic targets and association with GABA-immunoreactive structures. Synapse. 1998; 29:193–205. [PubMed: 9635889]

Chrobak JJ, Buzsaki G. Gamma oscillations in the entorhinal cortex of the freely behaving rat. J Neurosci. 1998; 18(1):388–398. [PubMed: 9412515]

de Curtis M, Paré D. The rhinal cortices: a wall of inhibition between the neocortex and the hippocampus. Prog Neurobiol. 2004; 74:101–110. [PubMed: 15518955]

DeFelipe J. Types of neurons, synaptic connections and chemical characteristics of cells immunoreactive for calbindin-D28K, parvalbumin and calretinin in the neocortex. J Chem Neuroanat. 1997; 14:1–19. [PubMed: 9498163]

DeFelipe J, Hendry SH, Jones EG. Synapses of double bouquet cells in monkey cerebral cortex visualized by calbindin immunoreactivity. Brain Res. 1989; 503:49–54. [PubMed: 2611658]

Dombrowski SM, Hilgetag CC, Barbas H. Quantitative architecture distinguishes prefrontal cortical systems in the rhesus monkey. Cereb Cortex. 2001; 11:975–988. [PubMed: 11549620]

Ellender TJ, Paulsen O. The many tunes of perisomatic targeting interneurons in the hippocampal network. Front Cell Neurosci. 2010; 4:26. [PubMed: 20740069]

Fan J, Byrne J, Worden MS, Guise KG, McCandliss BD, Fossella J, Posner MI. The relation of brain oscillations to attentional networks. J Neurosci. 2007; 27(23):6197–6206. [PubMed: 17553991]

Fell J, Klaver P, Lehnertz K, Grunwald T, Schaller C, Elger CE, Fernandez G. Human memory formation is accompanied by rhinal-hippocampal coupling and decoupling. Nat Neurosci. 2001; 4(12):1259–1264. [PubMed: 11694886]

Fiala JC. Reconstruct: A free editor for serial section microscopy. J Microsc. 2005; 218:52–61. [PubMed: 15817063]

Fiala JC, Harris KM. Cylindrical diameters method for calibrating section thickness in serial electron microscopy. J Microsc. 2001; 202:468–472. [PubMed: 11422668]

Fries P. A mechanism for cognitive dynamics: neuronal communication through neuronal coherence. Trends Cogn Sci. 2005; 9(10):474–480. [PubMed: 16150631]

Fries P, Reynolds JH, Rorie AE, Desimone R. Modulation of oscillatory neuronal synchronization by selective visual attention. Science. 2001; 291(5508):1560–1563. [PubMed: 11222864]

Fuchs EC, Zivkovic AR, Cunningham MO, Middleton S, Lebeau FE, Bannerman DM, Rozov A, Whittington MA, Traub RD, Rawlins JN, Monyer H. Recruitment of parvalbumin-positive interneurons determines hippocampal function and associated behavior. Neuron. 2007; 53(4):591–604. [PubMed: 17296559]

Ganeshina O, Berry RW, Petralia RS, Nicholson DA, Geinisman Y. Differences in the expression of AMPA and NMDA receptors between axospinous perforated and nonperforated synapses are related to the configuration and size of postsynaptic densities. J Comp Neurol. 2004a; 468:86–95. [PubMed: 14648692]

Ganeshina O, Berry RW, Petralia RS, Nicholson DA, Geinisman Y. Synapses with a segmented, completely partitioned postsynaptic density express more AMPA receptors than other axospinous synaptic junctions. Neurosci. 2004b; 125(3):615–623.

Geinisman Y, Morrell F, de Yoledo-Morell L. Axospinous synapses with segmented postsynaptic densities: a morphologically distinct synaptic subtype contributing to the number of profiles of ‘perforated’ synapses visualized in random sections. Brain Res. 1987; 423:179–188. [PubMed: 3676805]

Germuska M, Saha S, Fiala JC, Barbas H. Synaptic distinction of laminar specific prefrontal-temporal pathways in primates. Cereb Cortex. 2006; 16:865–875. [PubMed: 16151179]

Gonchar Y, Burkhalter A. Distinct GABAergic targets of feedforward and feedback connections between lower and higher areas of rat visual cortex. J Neurosci. 2003; 23:10904–10912. [PubMed: 14645486]

Gray CM, Singer W. Stimulus-specific neuronal oscillations in orientation columns of cat visual cortex. Proc Natl Acad Sci USA. 1989; 86(5):1698–1702. [PubMed: 2922407]

Greenough WT, West RW, DeVoogd TJ. Subsynaptic plate perforations: changes with age and experience in the rat. Science. 1978; 202:1096–1098. [PubMed: 715459]

Gundersen HJG, Bagger P, Bendtsen TF, Evans SM, Korbo L, Marcussen N, Moller A, Nielsen K, Nyengaard JR, Pakkenberg B, Sorensen FB, Vesterby A, West MJ. The new stereological tools: disector, fractionator, nucleator and point sample intercepts and their use in pathological research and diagnosis. APMIS. 1988; 96:857–881. [PubMed: 3056461]

Hendry SH, Jones EG, Emson PC, Lawson DE, Heizmann CW, Streit P. Two classes of cortical GABA neurons defined by differential calcium binding protein immunoreactivities. Exp Brain Res. 1989; 76:467–472. [PubMed: 2767197]

Hilgetag CC, Dombrowski SM, Barbas H. Classes and gradients of prefrontal cortical organization in the primate. Neurocomputing. 2002:44–46. 823–829.

Hoistad M, Barbas H. Sequence of information processing for emotions through pathways linking temporal and insular cortices with the amygdala. Neuroimage. 2008; 40:1016–1033. [PubMed: 18261932]

Howard, CV.; Reed, MG. Unbiased Stereology, three dimensional measurement in microscopy. Oxford: BIOS Scientific Publishers Limited; 1998.

Howard MW, Rizzuto DS, Caplan JB, Madsen JR, Lisman J, Aschenbrenner-Scheibe R, Schulze-Bonhage A, Kahana MJ. Gamma oscillations correlate with working memory load in humans. Cereb Cortex. 2003; 13(12):1369–1374. [PubMed: 14615302]

Insausti R, Amaral DG. Entorhinal cortex of the monkey: IV. Topographical and laminar organization of cortical afferents. J Comp Neurol. 2008; 509:608–641. [PubMed: 18551518]

Jutras MJ, Buffalo EA. Synchronous neural activity and memory formation. Curr Opin Neurobiol. 2010; 20(2):150–155. [PubMed: 20303255]

Jutras MJ, Fries P, Buffalo EA. Gamma-band synchronization in the macaque hippocampus and memory formation. J Neurosci. 2009; 29(40):12521–12531. [PubMed: 19812327]

Kajiwara R, Takashima I, Mimura Y, Witter MP, Iijima T. Amygdala input promotes spread of excitatory neural activity from the perirhinal cortex to the entorhinal-hippocampal circuit. J Neurophysiol. 2003; 89(4):2176–2184. [PubMed: 12611981]

Kennerley SW, Walton ME, Behrens TE, Buckley MJ, Rushworth MF. Optimal decision making and the anterior cingulate cortex. Nat Neurosci. 2006; 9:940–947. [PubMed: 16783368]

Klausberger T, Somogyi P. Neuronal diversity and temporal dynamics: the unity of hippocampal circuit operations. J Neurosci. 2008; 321(5885):53–57.

Kloosterman F, Van Haeften T, Witter MP, Lopes Da, Silva FH. Electrophysiological characterization of interlaminar entorhinal connections: an essential link for re-entrance in the hippocampal-entorhinal system. Eur J Neurosci. 2003; 18:3037–3052. [PubMed: 14656299]

Koganezawa N, Taguchi A, Tominaga T, Ohara S, Tsutsui K, Witter MP, Iijima T. Significance of the deep layers of entorhinal cortex for transfer of both perirhinal and amygdala inputs to the hippocampus. Neurosci Res. 2008; 61:172–181. [PubMed: 18407365]

Kondo H, Saleem KS, Price JL. Differential connections of the perirhinal and parahippocampal cortex with the orbital and medial prefrontal networks in macaque monkeys. J Comp Neurol. 2005; 493:479–509. [PubMed: 16304624]

Lavenex P, Amaral DG. Hippocampal-neocortical interaction: a hierarchy of associativity. Hippocampus. 2000; 10(4):420–430. [PubMed: 10985281]

Lavenex P, Suzuki WA, Amaral DG. Perirhinal and parahippocampal cortices of the macaque monkey: projections to the neocortex. J Comp Neurol. 2002; 447:394–420. [PubMed: 11992524]

Lavenex P, Suzuki WA, Amaral DG. Perirhinal and parahippocampal cortices of the macaque monkey: Intrinsic projections and interconnections. J Comp Neurol. 2004; 472:371–394. [PubMed: 15065131]

Le Van Quyen M, Staba R, Bragin A, Dickson C, Valderrama M, Fried I, Engel J. Large-scale microelectrode recordings of high-frequency gamma oscillations in human cortex during sleep. J Neurosci. 2010; 30(23):7770–7782. [PubMed: 20534826]

MacDonald AW 3rd, Cohen JD, Stenger VA, Carter CS. Dissociating the role of the dorsolateral prefrontal and anterior cingulate cortex in cognitive control. Science. 2000; 288(5472):2835–1838.

Makeig S, Delorme A, Westerfield M, Jung T, Townsend J, Courchesne E, Sejnowski TJ. Electroencephalographic brain dynamics following manually responded visual targets. PLoS Biol. 2004; 2(6):e176. [PubMed: 15208723]

Mann EO, Mody I. Control of hippocampal gamma oscillation frequency by tonic inhibition and excitation of interneurons. Nat Neurosci. 2010; 13(2):205–121. [PubMed: 20023655]

Manns JR, Eichenbaum H. Evolution of declarative memory. Hippocampus. 2006; 16(9):795–808. [PubMed: 16881079]

Medalla M, Barbas H. Diversity of laminar connections linking periarcuate and lateral intraparietal areas depends on cortical structure. Eur J Neurosci. 2006; 23:161–179. [PubMed: 16420426]

Medalla M, Barbas H. Synapses with inhibitory neurons differentiate anterior cingulate from dorsolateral prefrontal pathways associated with cognitive control. Neuron. 2009; 61(4):609–620. [PubMed: 19249280]

Medalla M, Barbas H. Anterior cingulate synapses in prefrontal areas 10 and 46 suggest differential influence in cognitive control. J Neurosci. 2010; 30(48):16068–16081. [PubMed: 21123554]

Medalla M, Lera P, Feinberg M, Barbas H. Specificity in inhibitory systems associated with prefrontal pathways to temporal cortex in primates. Cereb Cortex. 2007; 17(1):i136–i150. [PubMed: 17725996]

Middleton S, Jalic J, Kispersky T, Lebeau FE, Roopun AK, Kopell NJ, Whittington MA, Cunningham MO. NMDA receptor-dependent switching between different gamma rhythm-generating microcircuits in entorhinal cortex. Proc Natl Acad Sci USA. 2008; 105(47):18572–18577. [PubMed: 18997013]

Mohedano-Moriano A, Martinez-Marcos A, Pro-Sistiaga P, Blaizot X, Arroyo-Jimenez MM, Marcos P, Artacho-Pérula E, Insausti R. Convergence of unimodal and polymodal sensory input to the entorhinal cortex in the fascicularis monkey. Neurosci. 2008; 151:255–271.

Mohedano-Moriano A, Pro-Sistiaga P, Arroyo-Jimenez MM, Artacho-Pérula E, Insausti AM, Marcos P, Cebada-Sánchez S, Martínez-Ruiz J, Munoz M, Blaizot X, Martinez-Marcos A, Amaral DG, Insausti R. Topographical and laminar distribution of cortical input to the monkey entorhinal cortex. J Anat. 2007; 211:250–260. [PubMed: 17573826]

Moore CT, Wilson CG, Mayer CA, Acquah SS, Massari VJ, Haxhiu MA. A GABAergic inhibitory microcircuit controlling cholinergic outflow to the airways. J Appl Physiol. 2004; 96:260–270. [PubMed: 12972437]

Munoz M, Insausti R. Cortical efferents of the entorhinal cortex and the adjacent parahippocampal region in the monkey (Macaca fascicularis). Eur J Neurosci. 2005; 22:1368–1388. [PubMed: 16190892]

Murthy VN, Sejnowski TJ, Stevens CF. Heterogeneous release properties of visualized individual hippocampal synapses. Neuron. 1997; 18:599–612. [PubMed: 9136769]

Otte S, Hasenstaub A, Callaway EM. Cell type-specific control of neuronal responsiveness by gamma-band oscillatory inhibition. J Neurosci. 2010; 30(6):2150–2159. [PubMed: 20147542]

Paz R, Bauer EP, Paré D. Learning-related facilitation of rhinal interactions by medial prefrontal inputs. J Neurosci. 2007; 27:6542–6551. [PubMed: 17567815]

Paz R, Bauer EP, Paré D. Theta synchronizes the activity of medial prefrontal neurons during learning. Learn Mem. 2008; 15(7):524–531. [PubMed: 18612069]

Pelletier JG, Apergis J, Paré D. Low-probability transmission of neocortical and entorhinal impulses through the perirhinal cortex. J Neurophysiol. 2004; 91:2079–2089. [PubMed: 15069098]

Peters A, Palay SL. The morphology of synapses. J Neurocytol. 1996; 25:687–700. [PubMed: 9023718]

Peters, A.; Palay, SL.; Webster, HD. The fine structure of the nervous system Neurons and their supporting cells. New York: Oxford University Press; 1991.

Pinto A, Jankowski M, Sesack SR. Projections from the paraventricular nucleus of the thalamus to the rat prefrontal cortex and nucleus accumbens shell: ultrastructural characteristics and spatial relationships with dopamine afferents. J Comp Neurol. 2003; 459:142–155. [PubMed: 12640666]

Reiner A, Veenman CL, Medina L, Jiao Y, Del Mar N, Honig MG. Pathway tracing using biotinylated dextran amines. J Neurosci Methods. 2000; 103:23–37. [PubMed: 11074093]

Rempel-Clower NL, Barbas H. The laminar pattern of connections between prefrontal and anterior temporal cortices in the Rhesus monkey is related to cortical structure and function. Cereb Cortex. 2000; 10(9):851–865. [PubMed: 10982746]

Rosenmund C, Stevens CF. Definition of readily releasable pool of vesicles at hippocampal synapses. Neuron. 1996; 16(6):1197–1207. [PubMed: 8663996]

Rushworth MF, Buckley MJ, Behrens TE, Walton ME, Bannerman DM. Functional organization of the medial frontal cortex. Curr Opin Neurobiol. 2007; 17:220–227. [PubMed: 17350820]

Rushworth MF, Mars RB, Summerfield C. General mechanisms for making decisions? Curr Opin Neurol. 2009; 19(1):75–83.

Saleem KS, Kondo H, Price JL. Complementary circuits connecting the orbital and medial prefrontal networks with the temporal, insular, and opercular cortex in the macaque monkey. J Comp Neurol. 2008; 506:659–693. [PubMed: 18067141]

Schall JD, Stuphorn V, Brown JW. Monitoring and control of action by the frontal lobes. Neuron. 2002; 36:309–322. [PubMed: 12383784]

Sederberg PB, Kahana MJ, Howard MW, Donner EJ, Madsen JR. Theta and gamma oscillations during encoding predict subsequent recall. J Neurosci. 2003; 23(34):10809–10814. [PubMed: 14645473]

Seltzer B, Pandya DN. Afferent cortical connections and architectonics of the superior temporal sulcus and surrounding cortex in the rhesus monkey. Brain Res. 1978; 149(1):1–24. [PubMed: 418850]

Sirevaag AM, Greenough WT. Differential rearing effects on rat visual cortex synapses. II. Synaptic morphometry. Brain Res. 1985; 351:215–226. [PubMed: 3995348]

Sohal VS, Zhang F, Yizhar O, Deisseroth K. Parvalbumin neurons and gamma rhythms enhance cortical circuit performance. Nature. 2009; 459(7247):698–702. [PubMed: 19396159]

Somogyi P, Tamas G, Lujam R, Buhl EH. Salient features of synaptic organization in the cerebral cortex. Brain Res Brain Res Rev. 1998; 26:113–135. [PubMed: 9651498]

Stevens CF. Neurotransmitter release at central synapses. Neuron. 2003; 40:381–388. [PubMed: 14556715]

Suzuki WA. Encoding new memories and making them stick. Neuron. 2006; 50:19–21. [PubMed: 16600852]

Suzuki WA, Amaral DG. Topographic organization of the reciprocal connections between the monkey entorhinal cortex and the perirhinal and parahippocampal cortices. J Neurosci. 1994a; 14(3 Pt 2): 1856–1877. [PubMed: 8126576]

Suzuki WA, Amaral DG. Perirhinal and parahippocampal cortices of the macaque monkey: cortical afferents. J Comp Neurol. 1994b; 350(4):497–533. [PubMed: 7890828]

Suzuki WA, Zola-Morgan S, Squire LR, Amaral DG. Lesions of the perirhinal and parahippocampal cortices in the monkey produce long-lasting memory impairment in the visual and tactual modalities. J Neurosci. 1993; 13(6):2430–2451. [PubMed: 8501516]

Swanson LW, Köhler C. Anatomical evidence for direct projections from the entorhinal area to the entire cortical mantle in the rat. J Neurosci. 1986; 6:3010–3023. [PubMed: 3020190]

Tamas G, Szabadics J, Lorincz A, Somogyi P. Input and frequency-specific entrainment of postsynaptic firing by IPSPs of perisomatic or dendritic origin. Eur J Neurosci. 2004; 20(10): 2681–2690. [PubMed: 15548211]

Tomioka R, Rockland KS. Long-distance corticocortical GABAergic neurons in the adult monkey white and gray matter. J Comp Neurol. 2007; 505:526–538. [PubMed: 17924571]

Van Hoesen GW, Pandya DN. Some connections of the entorhinal (area 28) and perirhinal (area 35) cortices of the rhesus monkey. III. Efferent connections. Brain Res. 1975; 95(1):25–38. [PubMed: 1156867]

Van Hoesen GW, Pandya DN, Butters N. Cortical afferents to the entorhinal cortex of the rhesus monkey. Science. 1972; 175:1471–1473. [PubMed: 4622430]

Veenman CL, Reiner A, Honig MG. Biotinylated dextran amine as an anterograde tracer for single- and double-labeling studies. J Neurosci Methods. 1992; 41:239–254. [PubMed: 1381034]

Von Stein A, Sarnthein J. Different frequencies for different scales of cortical integration: from local gamma to long range alpha/theta synchronization. Int J Psychophysiol. 2000; 38(3):301–313. [PubMed: 11102669]

Walmsley B, Alvarez FJ, Fyffe RE. Diversity of structure and function at mammalian central synapses. Trends Neurosci. 1998; 21:81–88. [PubMed: 9498304]

Wang C, Ulbert I, Schomer DL, Marinkovic K, Halgren E. Responses of human anterior cingulate cortex microdomains to error detection, conflict monitoring, stimulus-response mapping familiarity, and orienting. J Neurosci. 2005; 25(3):604–613. [PubMed: 15659596]

Wang XJ. Neurophysiological and computational principles of cortical rhythms in cognition. Physiol Rev. 2010; 90(3):1195–1268. [PubMed: 20664082]

Wellman BJ, Rockland KS. Divergent cortical connections to entorhinal cortex from area TF in the macaque. J Comp Neurol. 1997; 389:361–376. [PubMed: 9414000]

Womelsdorf T, Fries P. The role of neuronal synchronization in selective attention. Curr Opin Neurobiol. 2007; 17:154–160. [PubMed: 17306527]

Womelsdorf T, Fries P, Mitra PP, Desimone R. Gamma-band synchronization in visual cortex predicts speed of change detection. Nature. 2006; 439:733–736. [PubMed: 16372022]

Zikopoulos B, Barbas H. Prefrontal projections to the thalamic reticular nucleus form a unique circuit for attentional mechanisms. J Neurosci. 2006; 26:7348–7361. [PubMed: 16837581]

Zikopoulos B, Barbas H. Parallel driving and modulatory pathways link the prefrontal cortex and thalamus. PLoS One. 2007; 2:e848.10.1371/journal.pone.0000848 [PubMed: 17786219]

Zola-Morgan S, Squire LR, Amaral DG, Suzuki WA. Lesions of perirhinal and parahippocampal cortex that spare the amygdala and hippocampal formation produce severe memory impairment. J Neurosci. 1989; 9(12):4355–4370. [PubMed: 2593004]

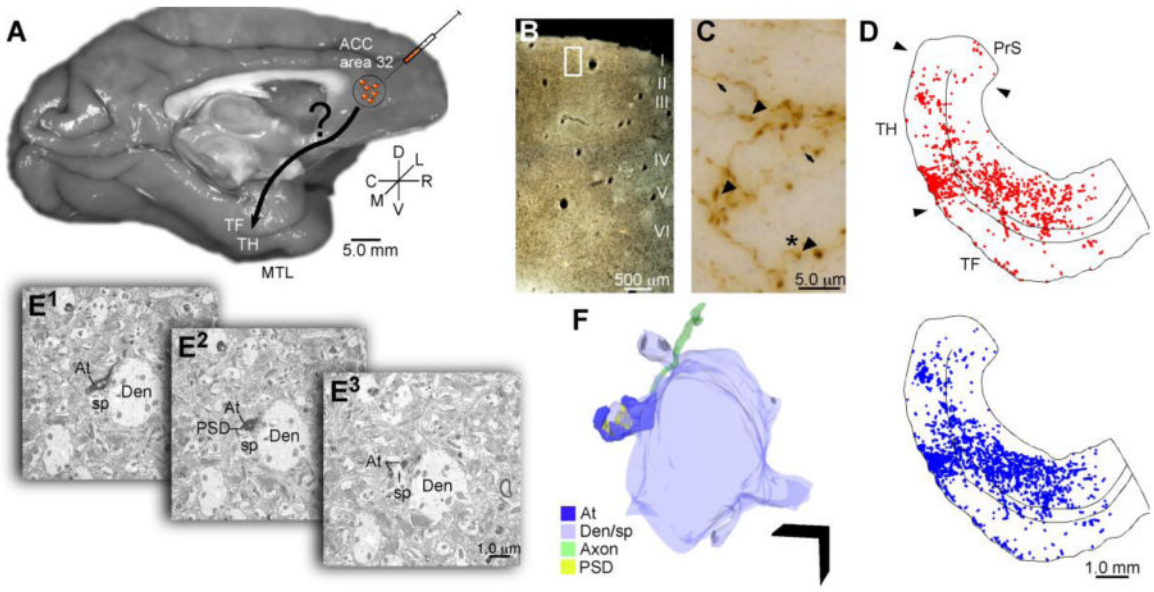

Figure 1.

Overview of experimental design. **A**, The anterograde tracer biotinylated dextran amine (BDA) or lucifer yellow (LY) was injected in ACC area 32 in rhesus monkeys (*Macaca mulatta*). **B, C, D**, Large (>0.97 μm) and small (≤0.97 μm) labeled boutons in the MTL were mapped and quantified in parahippocampal areas TH and TF using a combination of exhaustive sampling and stereological techniques (large boutons denoted by arrowheads in C, blue dots in D; small boutons denoted by arrows in C, red dots in D; the white rectangle in B shows the location of the image presented in C). Panel D is shown in complete coronal section in Figure 2B. **E, F**, Adjacent sections of tissue through the parahippocampal cortex were processed to view tracer label and the calcium binding proteins parvalbumin (PV) and calbindin (CB) using triple labeling immunohistochemistry and processed for electron microscopy. **E$^{1-3}$**, Serial ultrathin sections through labeled boutons and their postsynaptic targets were imaged at the EM level and reconstructed in 3D (**F**); Scale bar = 1 μm. Abbreviations: At: axon terminal; Den/sp: dendrite/spine; EM: electron microscope; PSD: postsynaptic density.

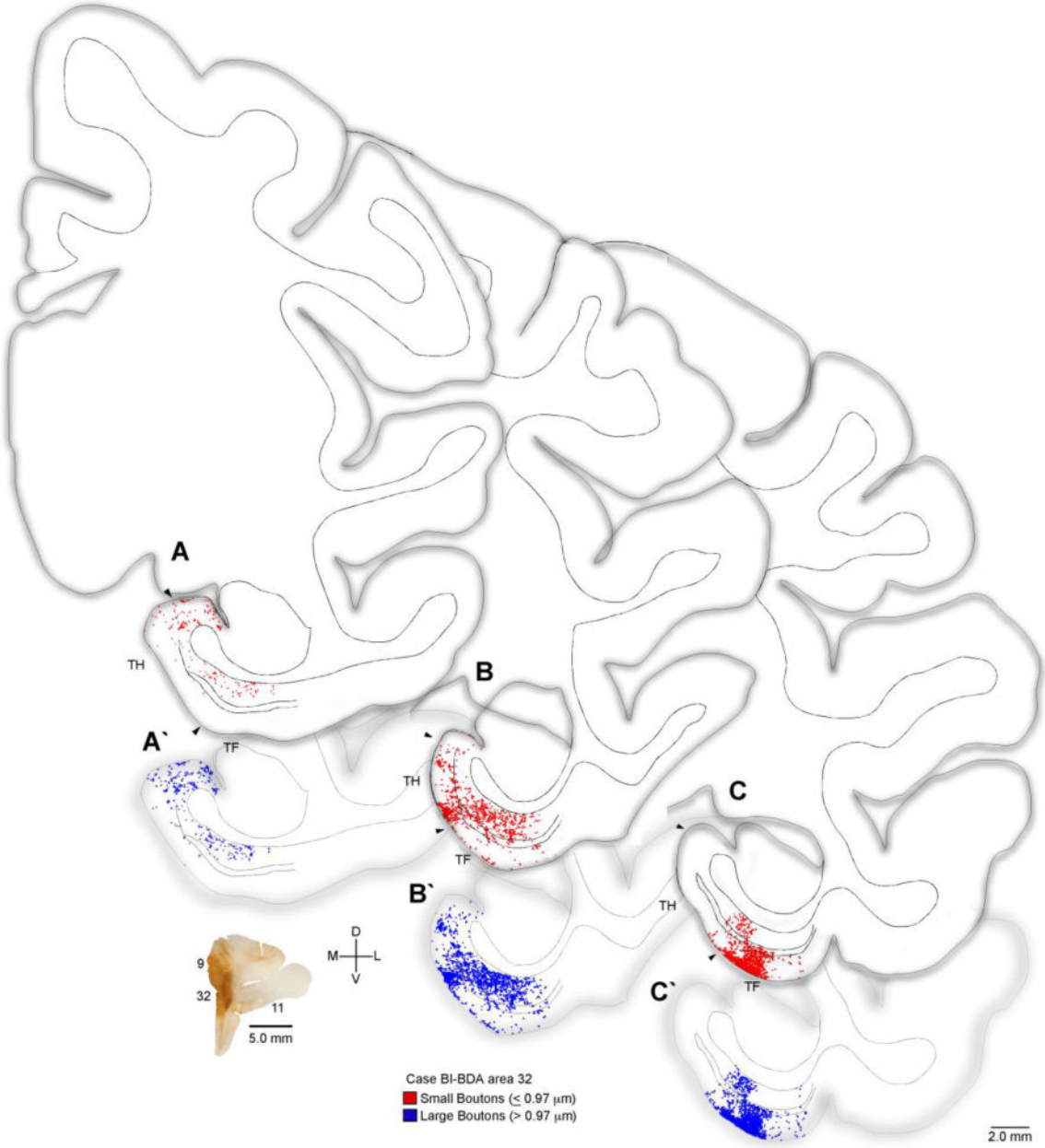

Figure 2.

Distribution of terminations from ACC to the parahippocampal cortices. Rostral (**A**) through caudal (**C**) tracings of coronal sections through parahippocampal cortices (areas TH, TF) of the rhesus monkey brain (Case BI) show the areal and laminar distribution of small (red) and large (blue) labeled boutons following injection of the anterograde tracer BDA in ACC area 32 (coronal section lower left). Double lines in the middle of the cortex denote layer IV. Abbreviations: ACC: anterior cingulate cortex; BDA: biotinylated dextran amine.

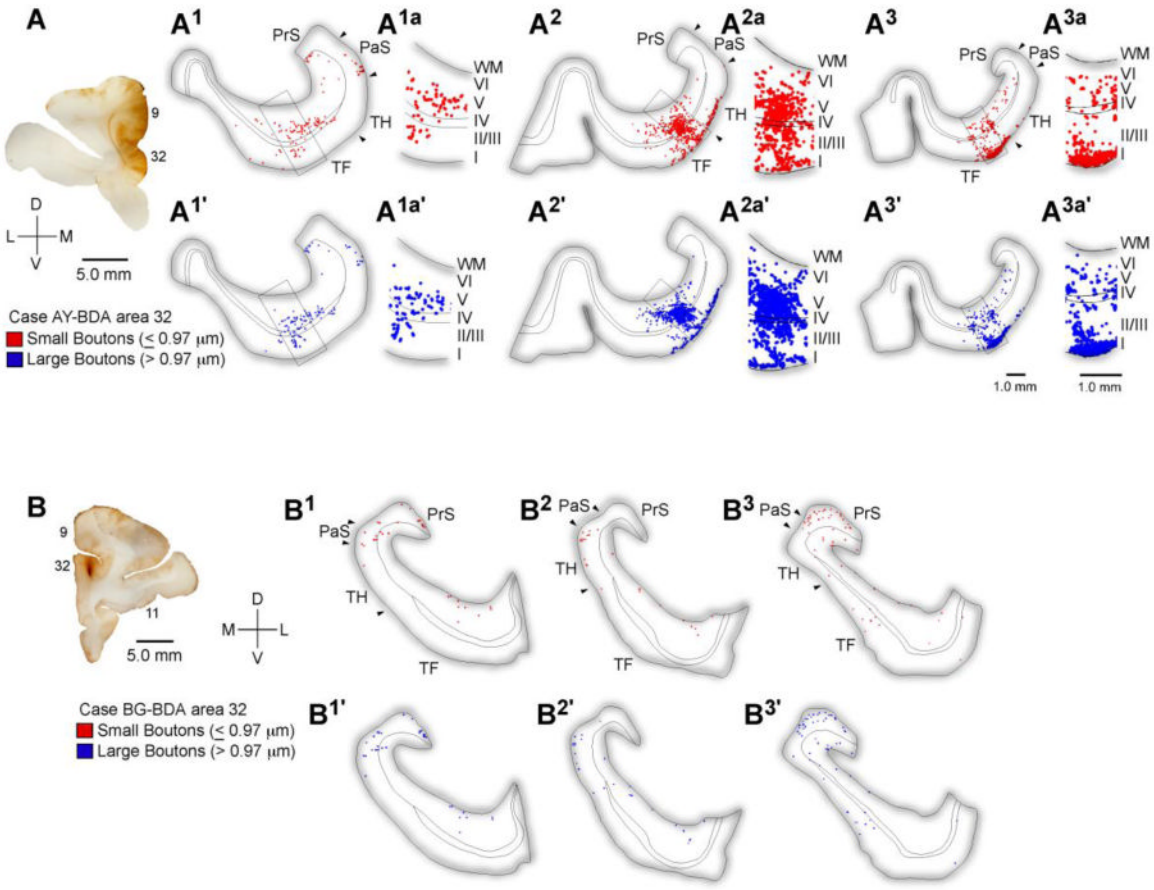

Figure 3.

Distribution of terminations from ACC to the parahippocampal cortices. **A**, Injection site in ACC area 32. **A$^{1\text{-}3a}$**, Rostral (**A^{1}**) through caudal (**A^{3}**) tracings of coronal sections through the parahippocampal areas TH and TF show the areal and laminar distribution of small (red) and large (blue) labeled boutons following injection of the anterograde tracer BDA in ACC area 32 (A, case AY) and the adjacent part of medial area 9. Higher magnification insets show the nearly even laminar distribution in the superficial and deep layers. **B**, Rostral through caudal tracings of coronal sections through the rhinal and parahippocampal cortices following a focal injection in area 32 (B, case BG). Abbreviations: ACC: anterior cingulate cortex; BDA: biotinylated dextran amine; PaS: parasubiculum; PrS: presubiculum; WM: white matter.

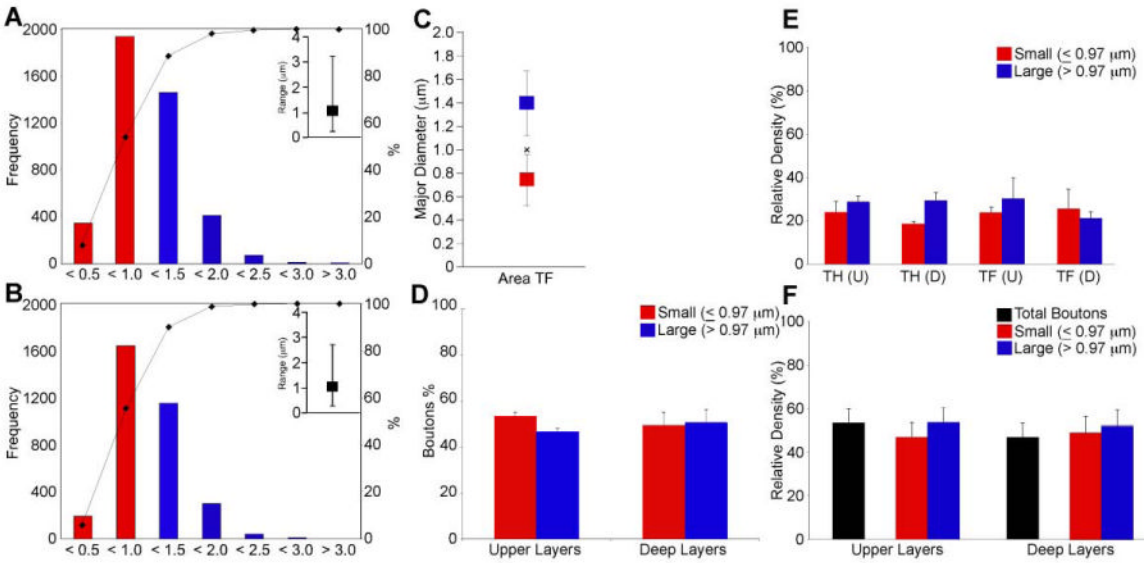

Figure 4.

Presynaptic characteristics of ACC (area 32) projections to MTL parahippocampal cortices. LM Analysis: **A, B**, Bouton major diameter frequency distributions in the superficial (A) and deep (B) layers of area TF following 2D analysis at the light microscope. Insets show the range of the distribution. **C**, Bouton major diameter clusters in area TF following 2D analysis at the light microscope. The average major diameter for distributions in the superficial and deep layers was equal to 1.0 μm (denoted by x). **D**, The ratio of large to small boutons, based on the values determined from the cluster analysis approached 50:50 in the superficial and deep layers of parahippocampal area TF following 2D analyses at the LM. **E**, Large and small boutons were about evenly distributed within the superficial and deep layers of parahippocampal areas TH and TF quantified using a combination of exhaustive sampling and stereological techniques. **F**, Relative densities of labeled boutons collapsed across parahippocampal areas. The even distribution of small and large boutons following exhaustive and stereological quantification at the LM is very similar to that observed following the 2D analysis at the LM (D). Abbreviations: ACC: anterior cingulate cortex; D: deep layers; LM: light microscope; U: upper layers.

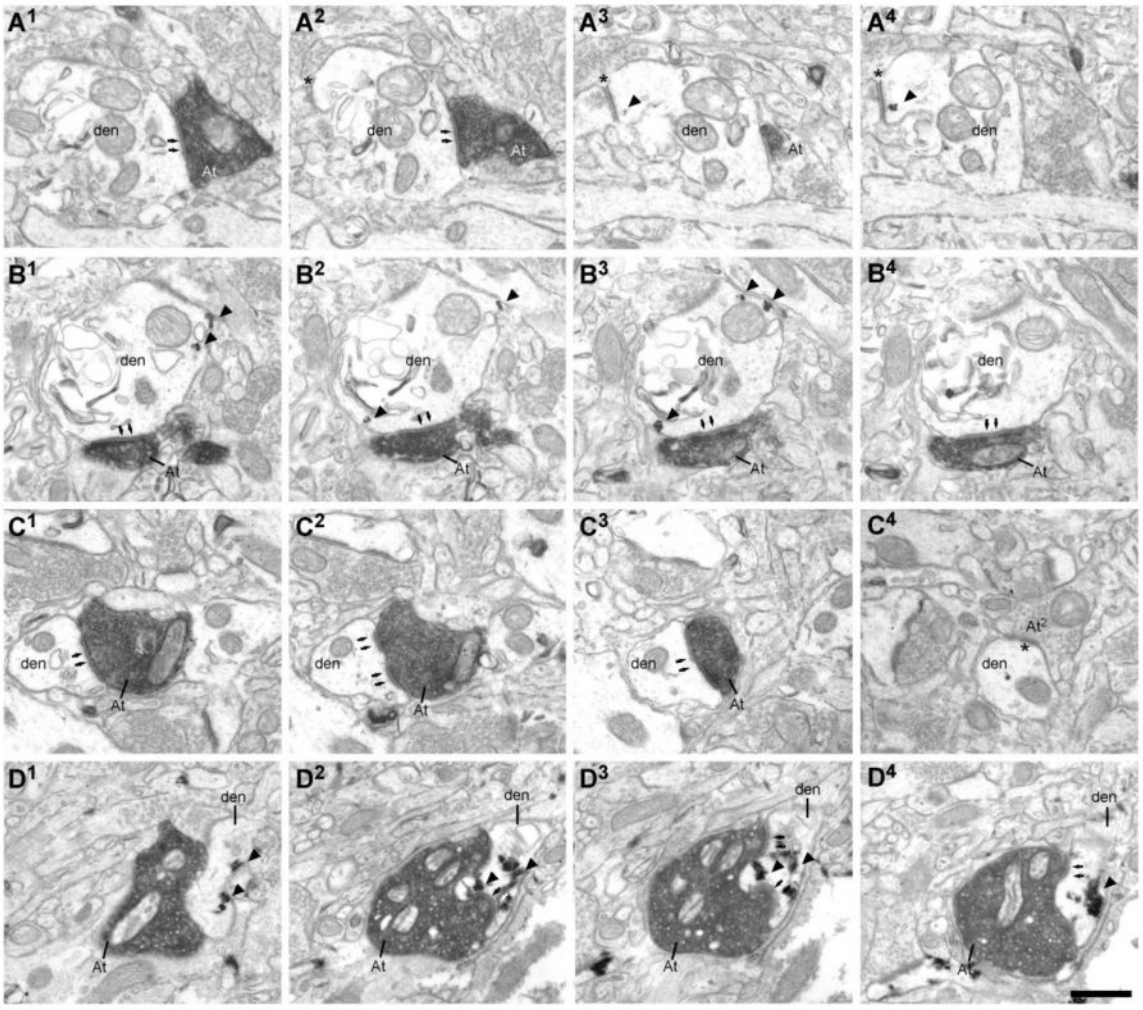

Figure 5.

Example of ACC (area 32) terminals forming synapses with presumed inhibitory neurons within the parahippocampal cortices. **A**, ACC boutons (At) forming synapses with parvalbumin (PV+) dendrites (den) in the upper and **B**, deep layers of the parahippocampal cortex. **A$^{1\text{-}4}$ & B$^{1\text{-}4}$**, Serial ultrathin sections show the postsynaptic densities (arrows). Note the gold signal showing immunoreaction for PV (arrowheads). Note the symmetrical synapse on the dendrite in A$^{2\text{-}4}$ (asterisk). C: ACC bouton forming a synapse with an unlabeled dendrite. **C$^{1\text{-}3}$**, Serial sections show the perforated PSD (arrows). **C^{4}**, The dendrite presented in C$^{1\text{-}3}$, followed through additional sections, shows a second shaft synapse (asterisk), found most frequently on inhibitory neurons. **D$^{1\text{-}4}$**, Serial ultrathin sections show a BDA labeled bouton forming a synapse with a CB expressing dendrite. Note the TMB signal showing immunoreaction for CB (arrowheads) and a perforated synapse (arrows) in D$^{2\text{-}4}$. Scale bars = 0.5 μm. Abbreviations: ACC: anterior cingulate cortex; BDA: biotinylated dextran amine; PSD: postsynaptic density; TMB: tetramethylbenzidine.

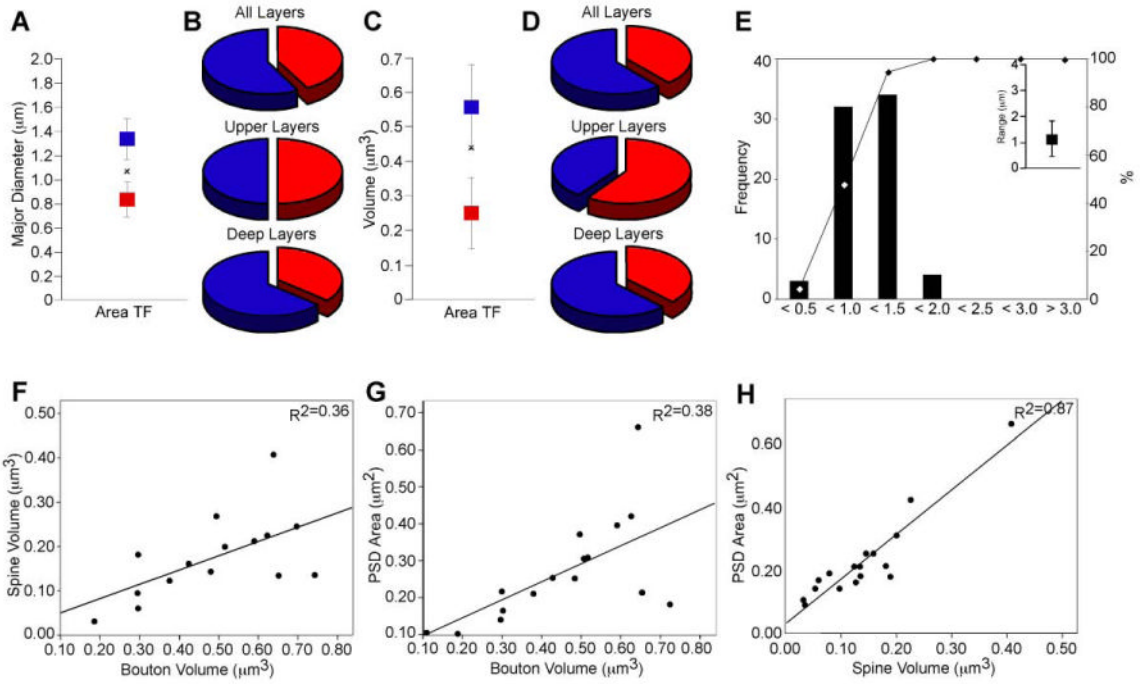

Figure 6.

Synaptic characteristics of ACC (area 32) boutons projecting to the parahippocampal cortices. EM analysis: **A**, Bouton major diameter clusters in area TF following 2D analysis at the EM. The average major diameter for the distribution was 1.1 μm (denoted by x). **B**, The ratio of large (blue) to small (red) boutons, based on the values determined from the cluster analysis, approached 50:50 in the superficial and was biased for more large boutons (blue) in the deep layers. **C,** Bouton volume clusters in area TF following 3D analysis at the electron microscope. The average volume for the distribution was equal to 0.44 μm^3 (denoted by x). **D**, The ratio of large (blue) to small (red) boutons, based on the values determined from the cluster analysis on the 3D data, approached 50:50 in the superficial and was biased for more large boutons (blue) in the deep layers. Note the similarity between B and D and the distribution of large and small boutons assessed at the light microscope (see Figure 4D-F). **E**, Bouton major diameter frequency distributions following 2D analysis at the EM. Inset shows the range of the distribution. Bouton frequency distribution quantified at the EM was similar to data obtained at the light microscope (see Figure 4A, 4B). **F**, Correlation between the size of presynaptic and postsynaptic sites for bouton volume and spine volume; and **G**, bouton volume and PSD area. **H**, There is a strong correlation between spine volume and PSD area. Abbreviations: ACC: anterior cingulate cortex; PSD: postsynaptic density.

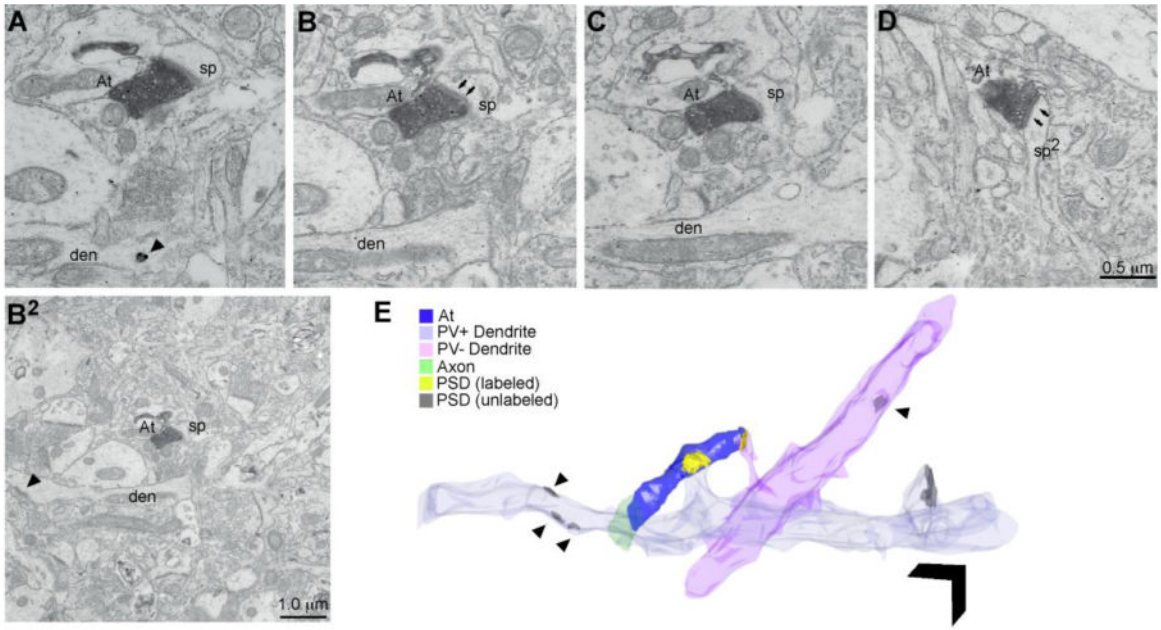

Figure 7.

Example of ACC (area 32) axon bouton forming synapses with inhibitory neurons within the MTL cortices. **A-D**, ACC bouton (At) forming synapses with both PV+ and PV-, sparsely spiny dendrites. **A, B**, Consecutive ultrathin sections show the postsynaptic density (PSD; arrows in B). The gold signal in the dendrite shows immunoreaction for PV in A (arrowhead). **B^2**, Wider view of the synapse presented in B. Note the PSD on the shaft of the PV+ dendrite (arrowhead). **C**, Ultrathin section shows that the postsynaptic spine emanates from the PV+ dendrite shown in A, B, & B^2. **D**, Ultrathin section shows the same bouton forming a second synapse with a spine from an unlabeled dendrite which also has shaft synapses (arrowhead in E associated with PV-dendrite), seen most frequently on inhibitory neurons. **E**, 3D reconstruction of the entire ultrathin series (58 consecutive, 67 nm thick sections) through the bouton and postsynaptic targets. Arrowheads denote synapses on the shaft of the dendrites. Scale bar = 1 μm. Abbreviations: ACC: anterior cingulate cortex; den: dendrite; MTL: medial temporal lobe; PV: parvalbumin; sp: spine.

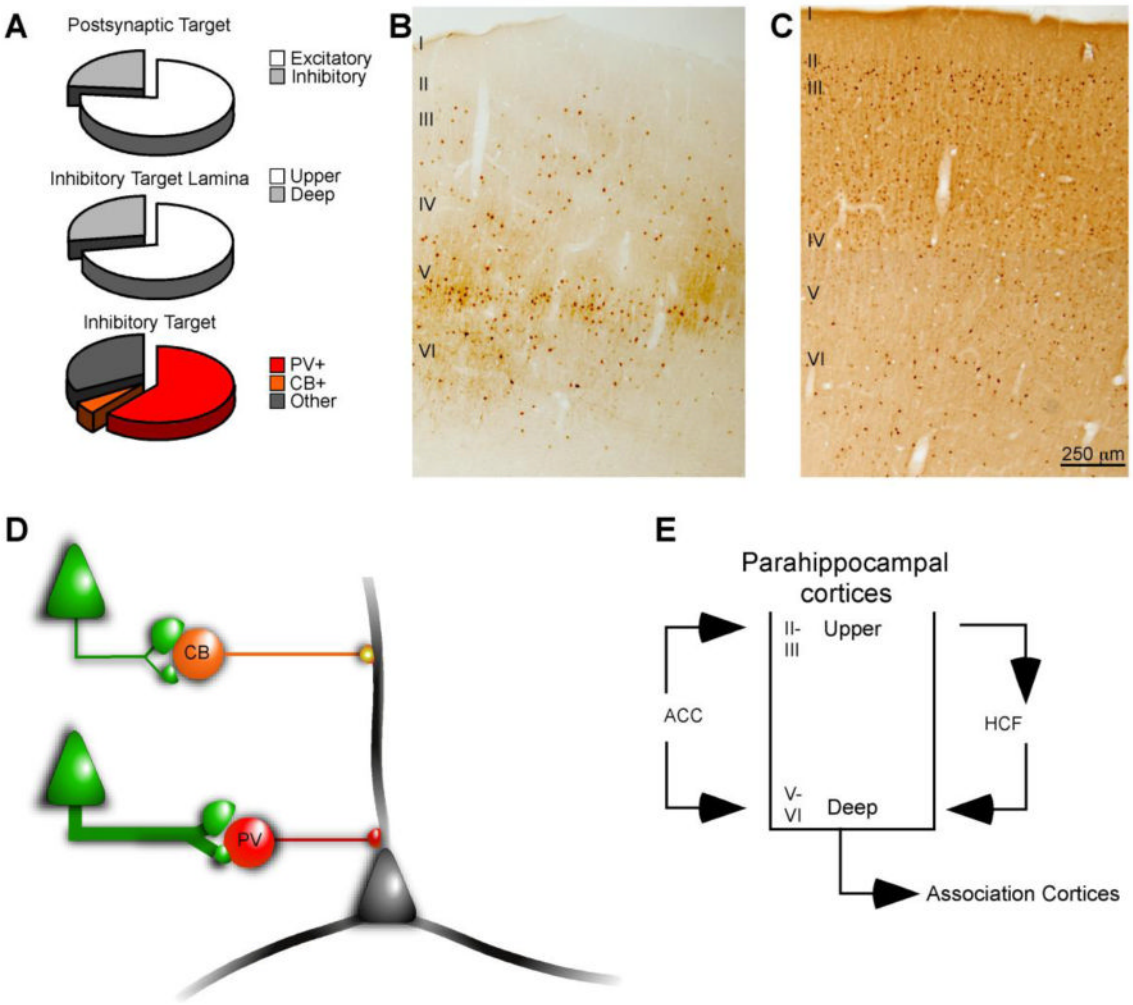

Figure 8.

Summary of postsynaptic targets of ACC area 32 projections to the parahippocampal cortices. **A**, The majority of ACC terminations formed synapses with postsynaptic elements of presumed excitatory neurons, but a significant number of ACC boutons targeted elements of presumed inhibitory neurons in the parahippocampal cortices. The majority of synapses formed with putative inhibitory targets were in the upper layers. Most of the inhibitory targets in the parahippocampal cortices were PV+, and very few were positive for CB. A moderate number of synapses were formed with unlabeled dendrites. **B, C**, PV (B) and CB (C) labeled neurons in parahippocampal area TF. The density of PV+ neurons is greatest in the middle-deep layers while CB labeled neurons are most prevalent in the upper layers. **D**, Schematic of ACC projections forming synapses with distinct neurochemical classes of presumed inhibitory neurons in the parahippocampal cortices. The prevalence of synapses is indicated by the thickness of the green line. PV+ inhibitory neurons target perisomatic elements, while CB+ inhibitory neurons form synapses at more distal parts of the dendritic arbor of local principal cells. **E**, Schematic illustration of the circuit linking the caudal mPFC in ACC with the hippocampal formation. ACC terminations are distributed throughout the upper and deep layers of the parahippocampal cortices which mediate information transfer to and from the hippocampal formation, respectively. Abbreviations:

ACC: anterior cingulate cortex; CB: calbindin; HCF: hippocampal formation; mPFC: medial prefrontal cortex; PV: parvalbumin.